Asociación Argentina
de Mecánica Computacional

Mecánica Computacional Vol XXIX, págs. 2785-2801 (artículo completo)
Eduardo Dvorkin, Marcela Goldschmit, Mario Storti (Eds.)
Buenos Aires, Argentina, 15-18 Noviembre 2010

# CONSIDERATION OF SIZE EFFECTS AND STRESS LOCALIZATION IN RESPONSE DETERMINATIONS USING THE DEM

**Luis E. Kosteski**[a], **Jorge D. Riera**[b], **Ignacio Iturrioz**[a]

[a]*PROMEC, Departamento de Engenharia Mecânica, Escola de Engenharia, Universidade Federal do Rio Grande do Sul, Porto Alegre, Brasil* <ignacio@mecanica.ufrgs.br, luiskosteski@hotmail.com>

[b]*Civil Engineering Department (DECIV), PPGEC, Universidade Federal do Rio Grande do Sul (UFRGS), Porto Alegre, RS, Brazil* < jorge.riera@ufrgs.br>

**Keywords:** Discrete elements, Numerical Analysis, Size Effect, Stress Localization, Fracture Mechanics, Brittle Materials

**Abstract**. In the truss-like Discrete Element Method (DEM) masses are considered lumped at nodal points and linked by means of unidimensional elements with arbitrary constitutive relations. In previous studies of the tensile fracture behavior of concrete cubic samples, it was verified that numerical predictions of fracture of non-homogeneous materials using DEM models are feasible and yield results that are consistent with the experimental evidence so far available. Applications that demand the use of large elements, in which extensive cracking within the elements of the model may be expected, require the consideration of the increase with size of the fractured area, in addition to the effective stress-strain curve for the element. This is a basic requirement in order to achieve mesh objectivity. Note that the degree of damage localization must be known *a priori*, which is a still unresolved difficulty of the non-linear fracture analysis of non-homogeneous large structures. Results of the numerical fracture analysis of 2D systems employing the DEM are reported in this contribution and compared with predictions based on the multi-fractal theory proposed by Carpinteri *et al* according to which a fractal dimension, contained in the interval (1,2), defines the fracture area for a unitary thickness. The assessment of the equivalence and ranges of validity of different approaches to account for size and strain rate effects appear today as one of the most urgent areas of study in the mechanics of materials. The influences of various parameters, such as the mesh size, the strain velocity and the shape of the fracture surface are assessed by means of numerical simulation. Methods employed in the homogenization of heterogeneous materials, in which damage is expected to occur with different level of stress localization, are also examined. Finally, conclusions on the performance of the numerical procedures employed in the reported studies are presented.

## 1 INTRODUCTION

In the truss-like Discrete Element Method (DEM) masses are considered lumped at nodal points and linked by means of unidimensional elements with arbitrary constitutive relations. In previous studies of the tensile fracture behavior of concrete cubic samples, it was verified that numerical predictions of fracture of non-homogeneous materials using DEM models are feasible and yield results that are consistent with the experimental evidence so far available. Applications that demand the use of large elements, in which extensive cracking within the elements of the model may be expected, require the consideration of the increase with size of the fractured area, in addition to the effective stress-strain curve for the element. This is a basic requirement in order to achieve mesh objectivity. Note that the degree of damage localization must be known *a priori*, which is a still unresolved difficulty of the non-linear fracture analysis of non-homogeneous large structures.

Results of the numerical fracture analysis of 2D systems employing the DEM are reported in this contribution and compared with predictions based on the multi-fractal theory proposed by Carpinteri et al. (1994) according to which a fractal dimension $\Delta$, contained in the interval (1,2), defines the fracture area per unit of thickness. The assessment of the equivalence and ranges of validity of different approaches to account for size and strain rate effects appear today as one of the most urgent areas of study in the mechanics of materials. The influences of various parameters, such as the mesh size, the strain velocity and the shape of the fracture surface are assessed by means of numerical simulation. Methods employed in the homogenization of heterogeneous materials, in which damage is expected to occur with different level of stress localization, are also examined. Finally, conclusions on the performance of the numerical procedures employed in the reported studies are presented.

## 2 THE TRUSS-LIKE DISCRETE ELEMENT METHOD

In the truss-like discrete element method (DEM) a continuum is represented by a set of lumped masses interconnected by a set of uni-axial elements or *bars*. In particular, Figure 1*a* and 1b show the discretization for a cubic system, for which the stiffness of the DEM elements corresponding to *an equivalent orthotropic linear elastic material* were obtained by Nayfeh and Hefzy (1978). The basic cubic module has 20 elements and 9 nodes. Every node has three degrees of freedom, namely the three components of the displacement vector in a global reference system. In case of an isotropic elastic material, the cross-sectional area $A_i$ of the longitudinal elements (those defining the edges of the module and those parallel to the edges connected to the node located at the centre of the module) in the equivalent discrete model is:

$$A_i = \phi\, L^2 \tag{1}$$

where $L$ is the length of the side of the cubic module under consideration. Similarly, the area $A_d$ of the diagonal elements is:

$$A_d = \frac{2}{\sqrt{3}}\,\delta\,\phi\, L^2 \tag{2}$$

Note that there is a difference in length between longitudinal and diagonal elements, since:

$$L = \left(2/\sqrt{3}\right) L_d \tag{3}$$

For approximately isotropic solids:

$$\phi = \left(9 + 8\delta\right) / \left(18 + 24\delta\right) \tag{4}$$

$$\delta = 9\nu\left(4 - 8\nu\right) \tag{5}$$

where $\nu$ is Poisson's ratio. It is important to point out that for $\nu = 0.25$, the correspondence between the equivalent discrete solid and the isotropic continuum is complete. On the other hand, for values of $\nu \neq 0.25$ small discrepancies appear in the shear terms, which may nevertheless be neglected. It is interesting to note that while no lattice or truss-like model can exactly represent a *locally* isotropic continuum, it can also be argued that no perfect *locally isotropic continuum exists* in the physical world. In fact, the continuum itself does not exist. Isotropy in solids is a bulk property that reflects properties of the random distribution of the orientation of the elements. The derivation of the areas of longitudinal and diagonal elements given for a cubic array by equations (1) and (2) may be found in Nayfeh and Hefzy (1978) and Dalguer et al. (2001).

The equations of motion are obtained from equilibrium conditions of all forces acting on the nodal masses, resulting a system of equations of the form:

$$\mathbf{M}\ddot{\mathbf{x}} + \mathbf{C}\dot{\mathbf{x}} + \mathbf{F}\left(t\right) - \mathbf{P}\left(t\right) = 0 \tag{6}$$

in which $\mathbf{x}$, $\dot{\mathbf{x}}$ and $\ddot{\mathbf{x}}$ denote vectors containing the nodal displacements, velocities and accelerations, respectively, while $\mathbf{M}$ and $\mathbf{C}$ are the mass and damping matrices. The vectors $\mathbf{F}\left(t\right)$ and $\mathbf{P}\left(t\right)$ contain the internal and external nodal loads.

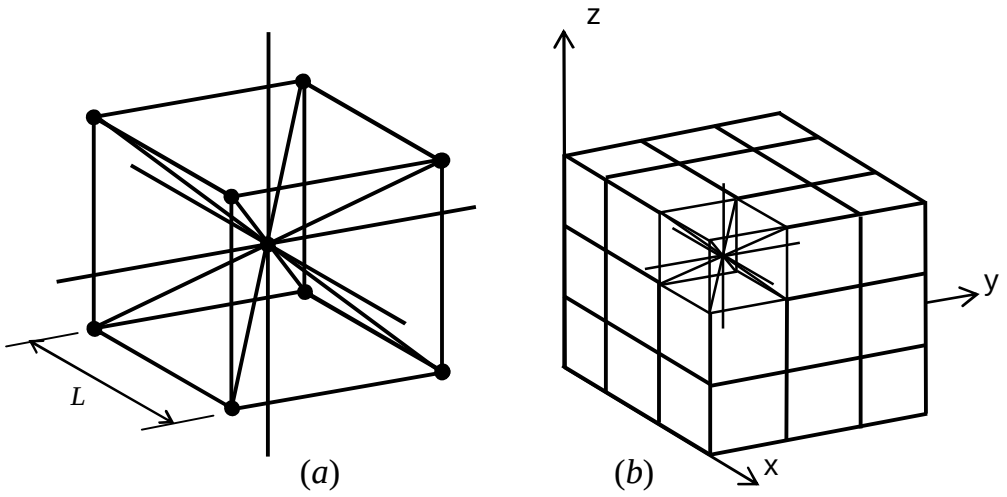


Figure 1: DEM discretization strategy: (a) basic cubic module, (b) generation of prismatic body.

Since matrices $\mathbf{M}$ and $\mathbf{C}$ are diagonal, the equations in expression (5) are not coupled, and they can be easily integrated in the time domain using an explicit finite difference scheme. It is worth noting that since nodal coordinates are updated at every time step, large displacements are accounted for naturally. Stability of the integration scheme is insured by adoting a time interval $\Delta t$ in the integration process such that:

$$\Delta t \leq \frac{0.6L}{C_\rho} \tag{7}$$

in which $C_\rho$ is the propagation velocity of longitudinal waves,

$$C_\rho = \sqrt{E/\rho} \tag{8}$$

The convergence of DEM solutions in linear elasticity and elastic instability problems was verified by Hayashi (1982) and Dalguer et al. (2001), among others.

## 3. NON-LINEAR CONSTITUTIVE MODEL FOR MATERIAL DAMAGE

Rocha et al. (1991) adopted the softening law to the quasi fragile materials proposed by Hilleborg (1978) extendeding the Discrete Element Model to handle fragile fracture by means of the bilinear constitutive relationship (ECR) shown in Figure 2, which allows accounting for the irreversible effects of crack nucleation and propagation, therefore, it predicts the reduction in the element load carrying capacity with damage. The area under the force vs. strain curve (the area of the triangle OAB in Figure 2) represents the energy density necessary to fracture the area of influence of the element. Thus, for a given point P on the force vs. strain curve, the area of the triangle OPC represents the *reversible* elastic energy density stored in the element, while the area of the triangle OAP is the energy density dissipated by damage. Once the damage energy density equals the fracture energy, the element fails and loses its load carrying capacity. On the other hand, in the case of compressive loads the material behavior is assumed linearly elastic. Thus, failure in compression is induced by indirect traction.

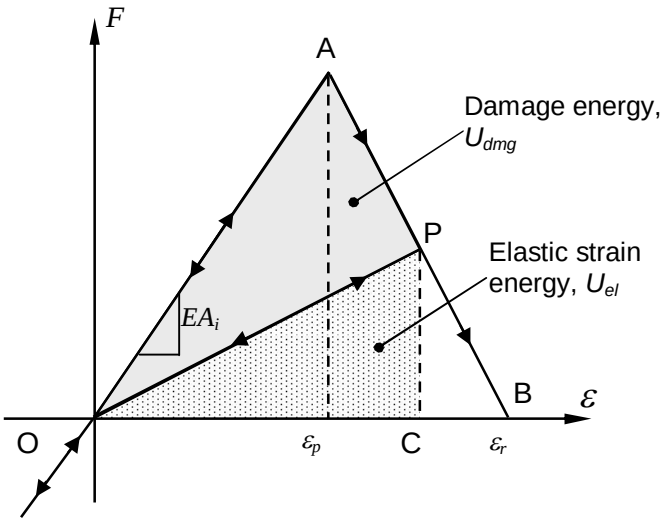


Figure 2: Bilinear constitutive law adopted for DEM uni-axial elements.

Constitutive parameters and symbols are shown in Figure 2 (see Rocha, 1989, and Rocha et al, 1991). The element axial force $F$ depends on the axial strain $\varepsilon$. The area associated to each element is given by equations (1) or (2) for longitudinal and diagonal elements, respectively. An e*quivalent fracture area* $A_i^*$ of each element is defined in order to satisfy the condition that the energies dissipated by fracture of the continuum and by its discrete representation are equivalent. With this purpose, fracture of a cubic sample of dimensions $L \times L \times L$ is considered. The energy dissipated by fracture of a continuum cube due to a crack parallel to one of its faces is:

$$\Gamma = G_f \Lambda = G_f L^2 \tag{9}$$

in which $\Lambda$ is the actual fractured area, *i.e.* $L^2$. On the other hand, the energy dissipated when a DEM module of dimensions $L \times L \times L$ fractures in two parts consists of the contributions of five

longitudinal elements (four coincident with the module edges and an internal one) and four diagonal elements, as shown in Figure 1a. Then, the energy dissipated by the DEM module can be written as follows:

$$\Gamma_{\text{DEM}} = G_f \left( 4 \cdot 0.25 \cdot c_A + c_A + 4 \cdot c_A \cdot \left( \frac{2}{\sqrt{3}} \right)^2 \right) L^2 \tag{10}$$

The first term between brackets accounts for the four edge elements, the second term for the internal longitudinal element, while the third term represents the contribution of the four diagonal elements. The coefficient $c_A$ is a scaling parameter used to establish the equivalence between $\Gamma$ and $\Gamma_{\text{DEM}}$. Thus:

$$G_f L^2 = G_f \left( \frac{22}{3} c_A \right) L^2 \tag{11}$$

from which it follows that $c_A$ = 3/22. Finally, the equivalent transverse fracture area of the longitudinal elements is

$$A_l^* = (3/22)\ L^2 \tag{12}$$

while for the diagonal elements is

$$A_d^* = (4/22)\ L^2 \tag{13}$$

The c*ritical failure strain* ($\varepsilon_p$) is defined as the largest strain attained by the element before the damage initiation (point A in Figure 2). The relationship between $\varepsilon_p$ and the specific fracture energy $G_f$ is given in terms of Linear Elastic Fracture Mechanics as:

$$\varepsilon_p = R_f \sqrt{\frac{G_f}{E\left(1-\nu^2\right)}} \tag{14}$$

in which $R_f$ is the so-called failure factor, which may accounts for the presence of an intrinsic defect of size *a*. $R_f$ may be expressed in terms of *a* as:

$$R_f = \frac{1}{Y\sqrt{a}} \tag{15}$$

in which *Y* is a dimensionless parameter that depends on both the specimen and crack geometry. The element loses its load carrying capacity when the *limit strain* $\varepsilon_r$ is reached (Point C in Figure 2). This value must satisfy the condition that, upon failure of the element, the dissipated energy density equals the product of the element fracture area $A_i^*$ times the specific fracture energy $G_f$, divided by the element length. Hence:

$$\int_0^{\varepsilon_r} F(\varepsilon) d\varepsilon = \frac{G_f \cdot A_i^*}{L_i} = \frac{K_r \cdot \varepsilon_p^2 \cdot E \cdot A_i}{2} \tag{16}$$

in which the sub index *i* is replaced by *l* or *d* depending on whether the element under consideration is a longitudinal or diagonal. The coefficient $K_r$ is a function of the material properties and the element length $L_i$:

$$K_r = \left(\frac{G_f}{E\varepsilon_p^2}\right)\left(\frac{A_i^*}{A_i}\right)\left(\frac{2}{L_i}\right) \tag{17}$$

In order to guarantee the stability of the algorithm, the condition $K_r \geq 1$ must be satisfied (Riera and Rocha, 1991). In this sense it is interesting to define the critical element length:

$$L_{cr} = 2\left(\frac{G_f}{E\varepsilon_p^2}\right)\left(\frac{A_i^*}{A_i}\right) \tag{18}$$

Moreover:

$$(A_l^*/A_l) = (3/22)/\phi \tag{19}$$

$$A_d^*/A_d) = (\sqrt{3}/11)/(\delta\phi) \tag{20}$$

In the special case of an isotropic continuum with $\nu = 0.25$, the value of the coefficients above are $\delta = 1.125$ and $\phi = 0.4$, which leads to $(A_l^*/A_l) \approx (A_d^*/A_d) \approx 0.34$. Thus, for practical purposes, a single value of the critical length can be used for longitudinal and diagonal elements. Therefore, the stability condition may be expressed as:

$$K_r = \frac{L_{cr}}{L_i} \geq 1 \quad \Rightarrow \; L_i \leq L_{cr} \tag{21}$$

Finally, the expression for the limit strain is:

$$\varepsilon_r = K_r \, \varepsilon_{p.} \tag{22}$$

Besides, it is worth noting that although the DEM uses a scalar damage law to describe the uniaxial behavior of the elements, the global model accounts for anisotropic damage since it possess elements orientated in the different spatial directions.

## 4. FRACTAL DIMENSION

The concept of fractal dimension introduced by Manderblot (1982) and adopted in the multi-fractal theory proposed by Carpinteri et al. (1994), is used herein for the assessment of fracture of quasi fragile materials. In Carpinteri's view, the fractal dimension $\Delta$, contained in the interval (2,3), defines the fracture area. Several approaches have been proposed to determine the fractal dimension $\Delta$ (Carpinteri et al., 1999) in experimental studies. In the present analysis, the fracture surfaces are obtained by numerical simulation, employing the failure criteria previously described

In the so-called *patchwork* method, identified in this paper as Method 1, the fracture surface is approximated by plane triangles. The *patchwork* fractal dimension $\Delta_{patch}$, originally defined by Clarke (1986), is then obtained from the rate of divergence of the apparent area $A$ (the total area of the triangles) as the size of the surface elements decreases. In other words, the patchwork method aims at evaluating the same limit value, i.e. the fractal dimension, by approximating it from a different path. Thus, as the covering grid size decreases, then the apparent area $A$ increases (while the nominal area remains constant). By increasing resolution, more and more details are counted, which confirms the scale dependent nature of the Euclidean description:

$$\Delta_{patch} = 2 - \lim_{r \to 0} \frac{\log A(r)}{\log r} \tag{23}$$

In which $A$ is the apparent area and $r$ a characteristic length of discretization. In the 2D plate, employed in the examples in Section 5, equation (23) should be replaced by:

$$\Delta_{patch} = 1 - \lim_{r \to 0} \frac{\log \ell(r)}{\log r} \tag{24}$$

In which $\ell$ is a normalized length and $r$ the size of the discretization segments. An alternative approach applicable to a 2D domain is proposed herein and identified as Method 2; Let $\ell_0$ denote the reference length, which is divided in $n$ intervals of size $r$. In such case the actual length of the fracture may be written as:

$$\ell = n^{\Delta} r \tag{25}$$

In which $\Delta$ is a new estimate of the fractal dimension. It is clear that:

$$\frac{\ell}{\ell_0} = \frac{n^{\Delta} \cdot r}{n \cdot r}, \quad \frac{\ell}{\ell_0} = n^{\Delta - 1}, \quad (\Delta - 1) \log n = l \log\left(\ell / \ell_0\right) \tag{26}$$

From which the following expression follows:

$$\Delta = 1 + \frac{\log\left(\ell / \ell_0\right)}{\log n} \tag{27}$$

A third procedure to assess the fractal dimension, designated in this paper as Method 3, involves the fracture energy dissipated in the process. According to basic principles of LEFM and maintaining the notation of the previous approach, the minimum energy $U_{min}$ needed to split the plate under consideration in two parts would be given by equation (28), while the energy spent by fracture is defined by equation (29):

$$U_{min} = G_f \, n \, r \tag{28}$$

$$U_{num} = G_f \, n^{\Delta e} \, r \tag{29}$$

Combining equations (28) and (29) leads to the following expression for the fractal dimension $\Delta e$:

$$\Delta e = 1 + \frac{l \log\left(U_{num} / U_{\min}\right)}{\log n} \tag{30}$$

Expressions (27) and (30) constitute sound fractal dimension estimates if the length of discretization $r$ is equal or less than the characteristic dimension of the random field that defines the material properties. Note that in this paper the specific fracture energy random field is defined by a Weibull distribution.This approach to measure energy was employed earlier by Miguel et al. (2010) in the determination of fractal dimension of concrete cubic samples.

Finally, the fractal dimension of the fracture surfaces may also be calculated by a three-dimensional spectral method, specifically designed for self-affine sets (Turcotte, 1992; Carpinteri et al., 1999). It is based on the two-dimensional Fourier Transform Hst of the fracture relief. The method provides the fractal dimension as a function of the mean spectral power, but it will not be resorted to in the present paper. A still unresolved issue in the determination of fractal dimensions is related to multiple fractures, which are likely to occur,

for example, under high train rates.

## 5 EXAMPLES

Simulated rock plate samples under plane stress, fixed at their lower boundary and subjected to tension along their upper face were analyzed up to failure by numerical integration in the time domain. The sizes of the samples range from 1.0 to 15.0m (see Figure 3). The smallest DEM array that leads to satisfactory results consists of 10×10×1 cubic modules, with 1026 DOF, used for the 1.0m plate, while the 15.0m plate model consists of 150×150×1 cubic modules, with 204306 DOF, constituting the largest array used in this study. In all cases boundary displacement in the vertical direction were applied on the plate in order to simulate a Plane Strain test in the examples. Table 1 shows the basic dimensions of the four samples analyzed, while relevant material properties are given in Table 2.

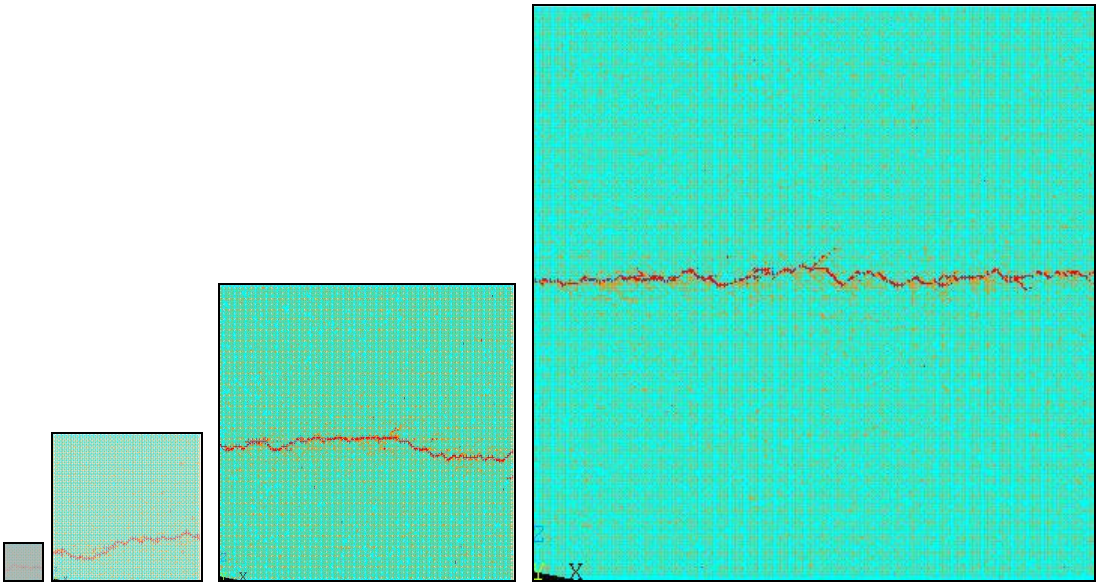

Figure 3: View of fracture configuration of 1, 4, 8 and 15m simulated plates

| Plates | | L |
|---|---|---|
| Plate 1.0 | (10×10) | 1.0m |
| Plate 4.0 | (40×40) | 4.0m |
| Plate 8.0 | (80×80) | 8.0m |
| Plate 15.0 | (150×150) | 15.0m |

Table 1: Rock plates dimensions (Lo = 0.10m).

| Properties | Value |
|---|---|
| $E$ (Young's modulus) | 7.5E10N/m$^2$ |
| $\rho$ (specific mass) | 2700kg/m$^3$ |
| $\nu$ (Poisson coefficient) | 0.25 |
| E($G_f$) (Expected value of specific fracture energy) | 1300N/m |
| CV($G_f$) (coeficient of variation of $G_f$ ) | 40% |
| $\varepsilon_p$ (critical strain) | 1.054E-4 |

Table 2: Material properties of rock (granite).

In loading case A, the nodes on the upper face of the specimens were subjected to controlled uniform displacements that smoothly increase from zero to a limit value, inducing a nominally uniform tension in the specimen. In loading case B prescribed forces were applied on the upper face, which increase with time at a constant rate until a perceptible jump in the total kinetic energy of the plate is detected, indicating the onset of nucleation. At that point the loading rate is set equal to zero, an integration proceeds under constant loading with a high damping to curb spurious vibrations. Six simulations were carried out for each loading case and for each plate size. For illustration purposes, the resulting stress-strain curves for all simulations for the 4.0 m plate are shown in Figure 4, for loading case A. Note that the specific fracture energy $G_f$ is also modelled as a random field with the properties indicated in Table 2, so each simulation leads to a different strength and a different stress-strain curve. The probability distribution of $G_f$ was assumed Weibull. The mean curve for all simulations is also shown in Figure 4. The mean curves for all tested sizes are shown in Figure 5, and also the scale effect in terms of global strain and stress results are shown in Figure 6.

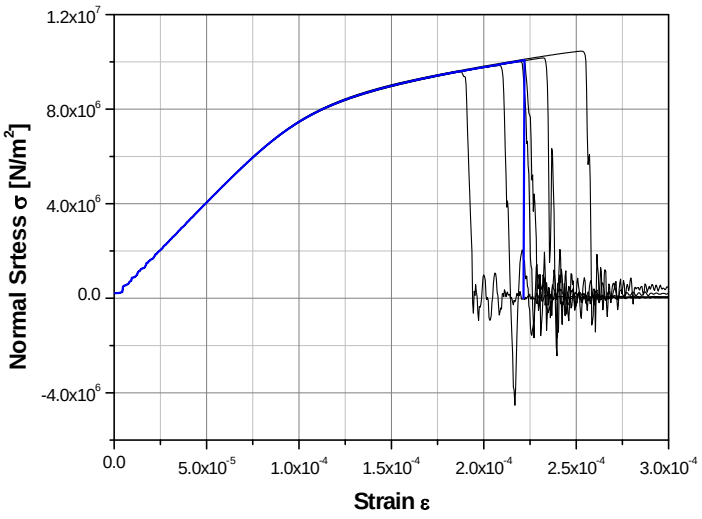


Figure 4: Mean vertical stress at lower support vs mean strain for the 4m rock plate. The results of six simulations and the average curve (in blue) are shown (case A – prescribed displacements).

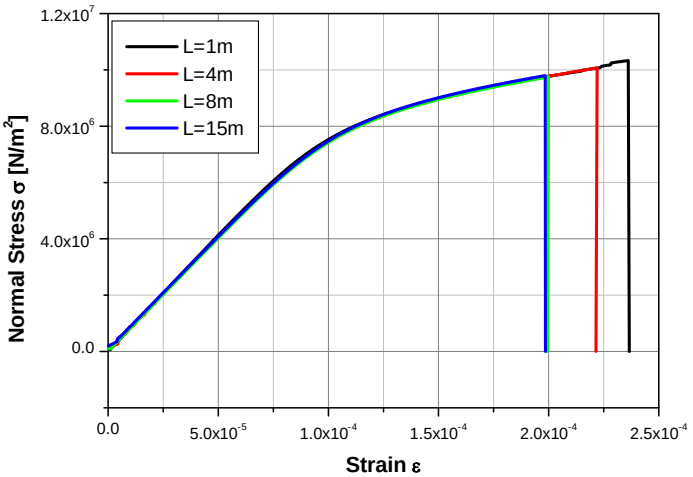


Figure 5: Mean vertical stress at lower support vs mean strain for the all plate sizes (case A – prescribed displacements).

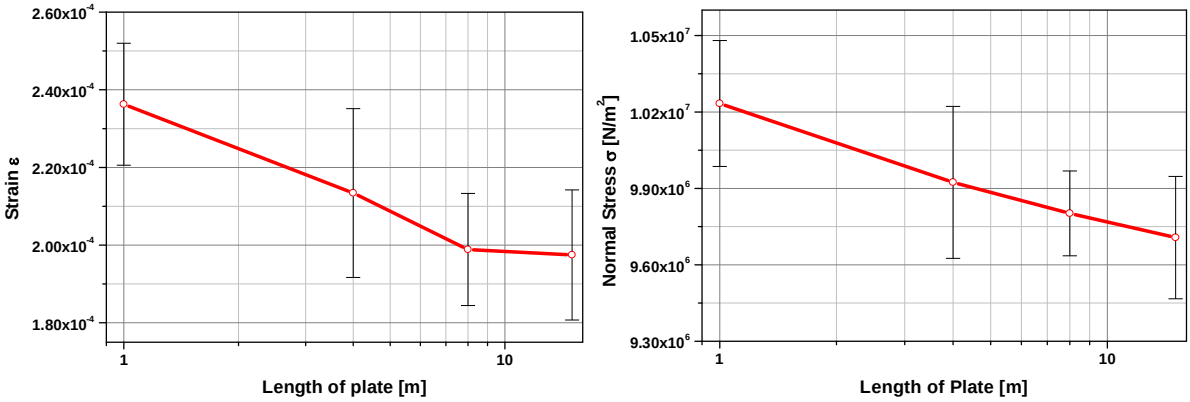


Figure 6: Variation of mean ultimate stress and strain with plate size (Logarithmic scale). The one standard deviation range of the simulations is also shown. (case A – prescribed displacements).

Typical cracked granite plates for loading Case A and Case B are shown in Figure 7. Colors cyan, orange and red represent undamaged, damaged and totally broken (failed) elements, respectively.

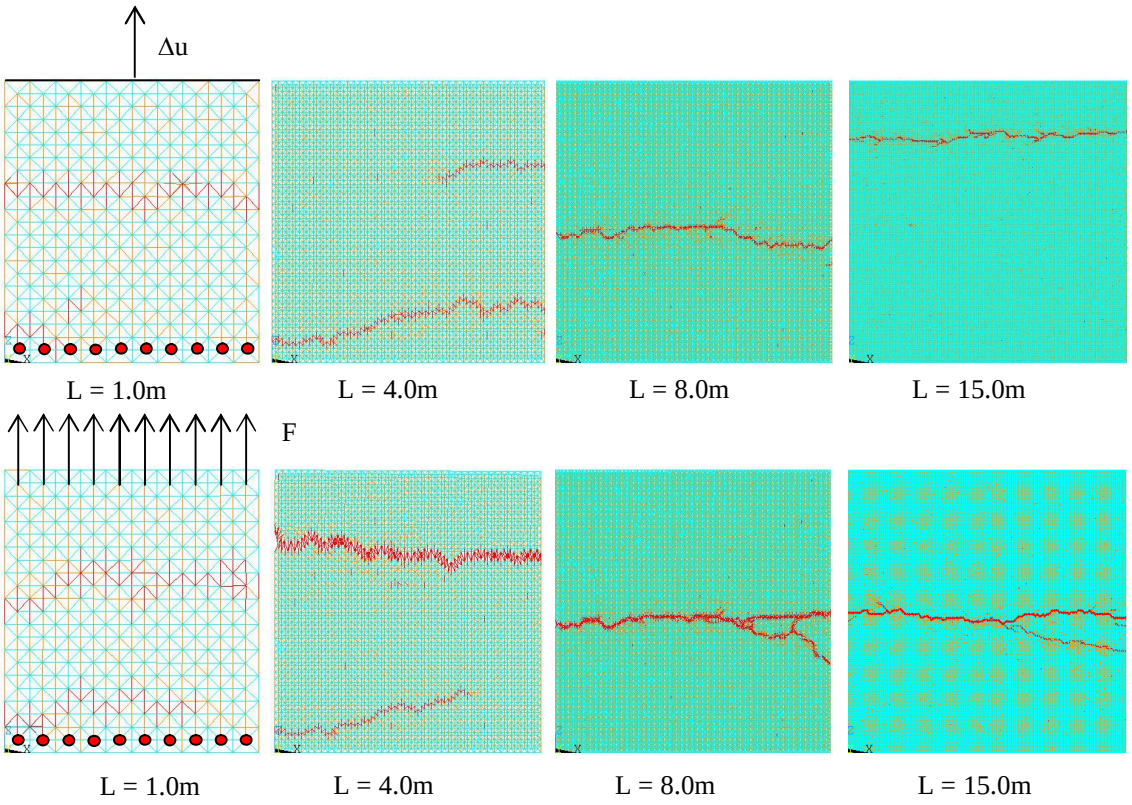


Figure 7: Rupture configuration of plates of various sizes subjected to applied displacements (above) (case A) and applied stresses (below) (case B). The simulated plate random properties are the same in both cases.

## 6 DETERMINATION OF FRACTAL DIMENSION FOR SIMULATED SAMPLES

The samples of the plates described in Section 5 were subjected to assessment employing methods 1 to 3 discussed in Section 4, in order to determine the fractal dimension of the fractured area.

In connection with the patchwork approach (Method 1), Figure 8, in which $x$ denotes the length of the discretization segments, shows the estimated values of $\Delta_{patch}$ for one of the simulations of the 4m plate. An estimate of $\Delta_{patch}$ is given by the limit as $x$ decreases (Carpinteri et al., 1999). It is important to note that when a fracture presents a bifurcation, the length in equation (24) was computed as the sum of the lengths of all fractures.

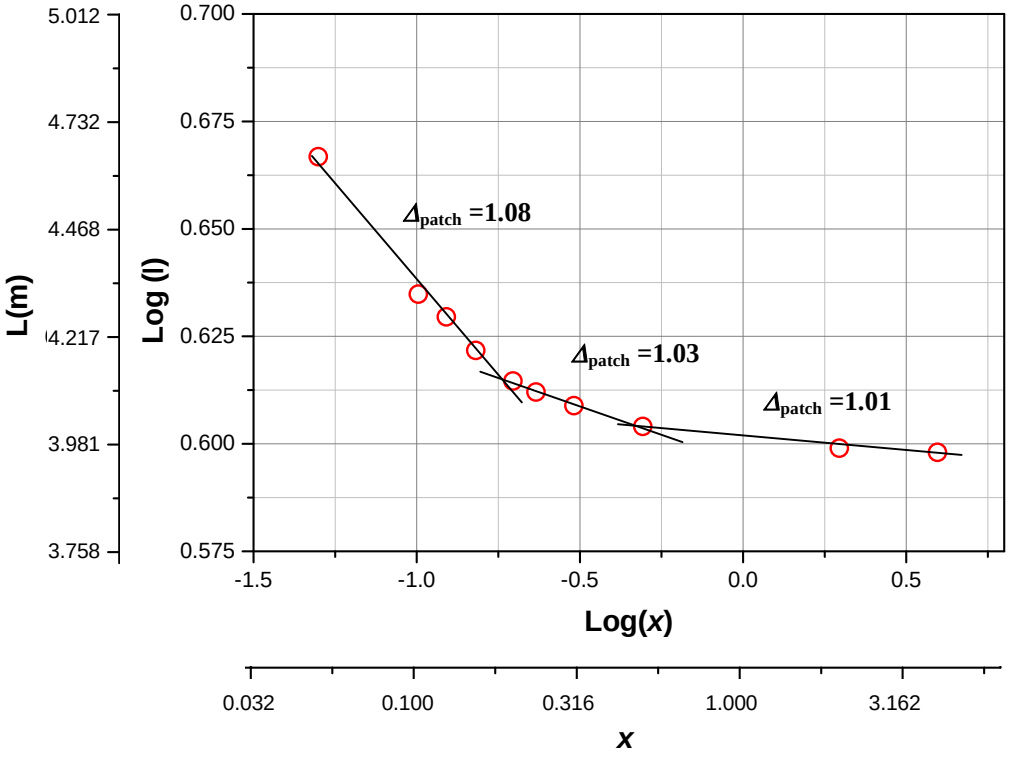


Figure 8: Log-log diagram of ℓ vs $x$ for one simulation of a 4m plate. All the dimensions are in meters

The fractured length ℓ, used in Methods 1 and 2, was measured in two different ways. First the centroids of broken diagonals elements were identified and linked to other groups of points whenever the distance to the nearest point in the group was less than the module length $L$. Only diagonals bars were considered to simplify the identification process without significantly affecting the resulting surface or length, designated $L_1$. Figure 9 shows (*a*) failed bars in a 1 m plate under stress with two cracks, (*b*) the position of the centroid of broken diagonal bars and (*c*) the grouping of these points in two different fractures. This grouping is performed by the program on the basis of the distances between points. Individual fractures with total length shorter than 10% of the plate length are neglected. To determine the actual location of the fracture surface (for fractures propagating in the x-direction), when more than one point present the same x-coordinate, the *z*-coordinate of the fracture is determined by the average of the *z*-coordinates of failed elements. Note that the fracture intersections with the plate faces do not necessarily coincide and thus have slightly different lengths. The length ℓ of the crack was determined as the average of the two lengths. The comparison between the DEM fracture configuration and the fissure surfaces obtained with the proposed methodology is shown in Figure 10.

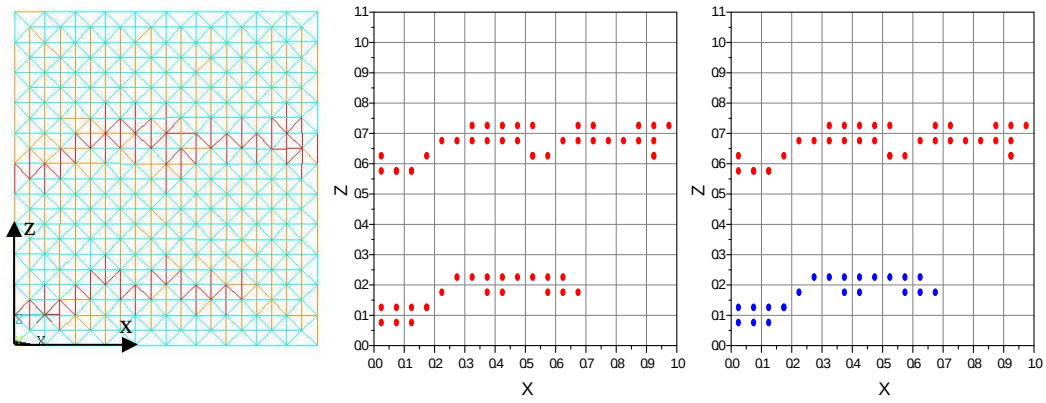


Figure 9: *a*) failure configuration of a 1 m plate with two cracks analyzed with DEM, *b*) identification of the centroid of broken diagonals bars and *c*) grouping of these points in different fractures.

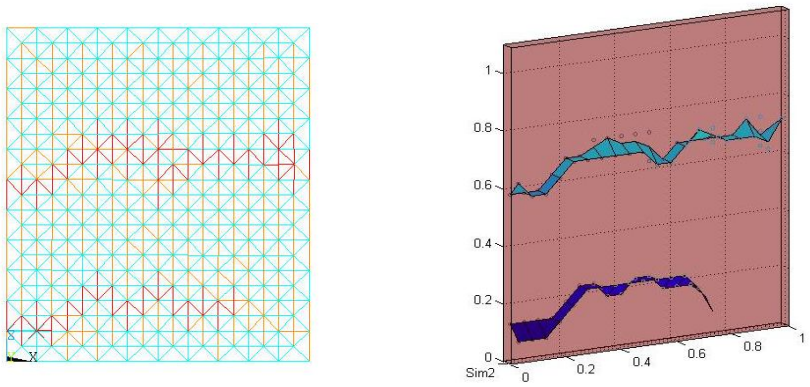


Figure 10: Comparison between the DEM rupture configuration and the fracture surfaces determined with post process analysis.

The process implemented to determine fracture lengths breaks down when branching occurs, in which case identification of the fracture surface must be done by visual inspection. Figure 11 shows, as an example, six simulations for the 1m plate and the failure surfaces generated in post- processing. The fifth simulation presents a bifurcation.

The second method to assess the fracture length, leading to measure $L_2$, consisted of adding coefficients $A_i^*$ of the all broken elements and dividing by the plate side length. While $L_1$ tends to measure only *macro* cracks, $L_2$ includes also small cracks and isolated damage. Thus, the condition $L_2 \geq L_1$ is always satisfied. Substituting these lengths in eq. (24) and (27) the fractal coefficients according to Method 1 and 2 may be obtained.

Method 3 takes into account macro cracks, smaller and isolated cracks, as well as micro cracks. This is because damaged elements also contribute to the dissipated energy. Figure 12 shows ($U_{num}/U_{min}$), *i.e.* the damage work normalized by the minimum energy needed to split the plate in two parts for Simulation 1 for the 1m plate (Load Case B). Note that $U_{min}$=1m×0.1m×1300N/m (length × thickness × fracture energy). After the plate is completely broken, the damage work ceases growing. For simulation 1, $U_{num}/U_{min}$ =1.377, which leads to $\Delta e$ = 1.139.

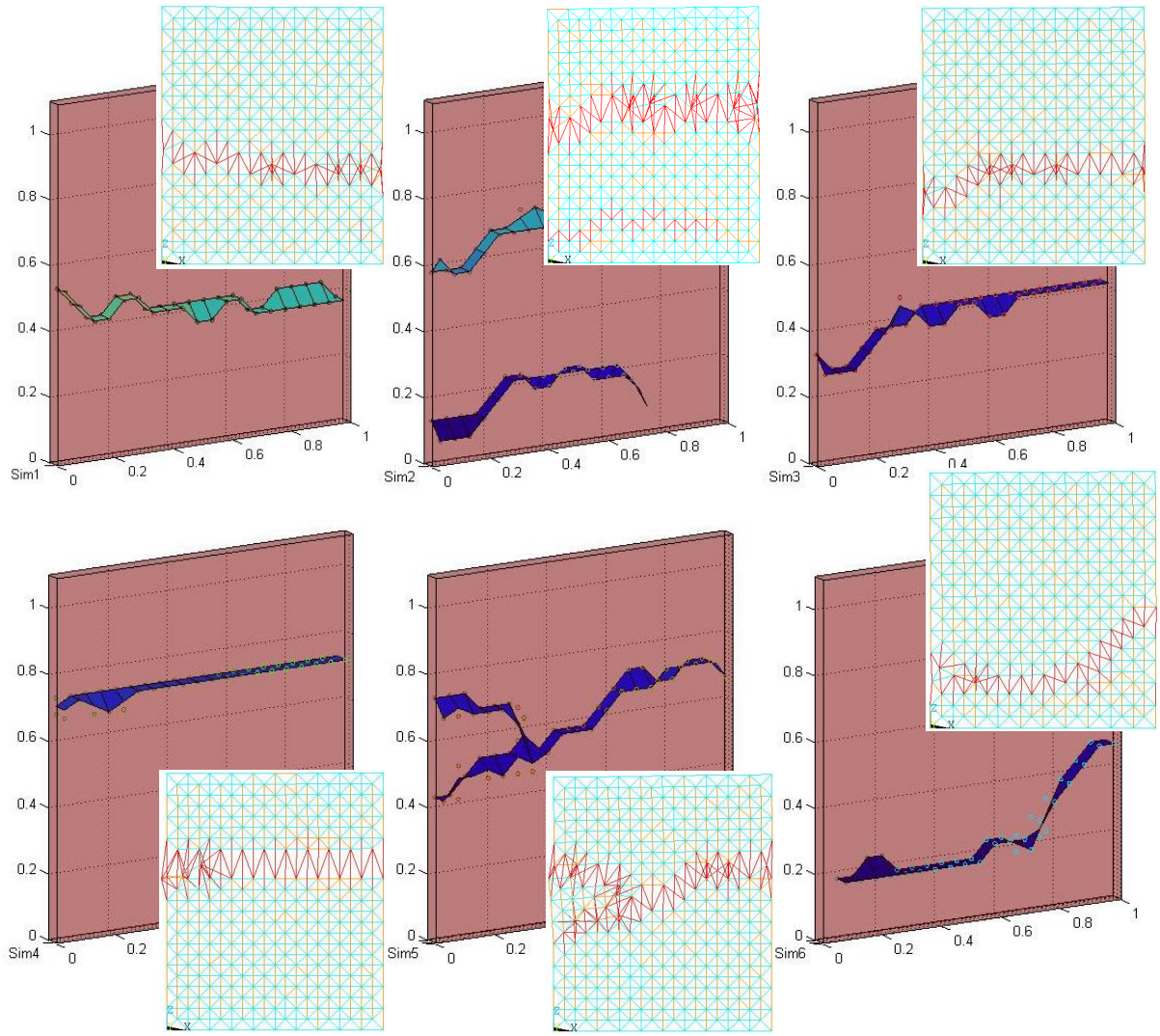


Figure 11: Final configurations obtained with the DEM for six simulations of 1m plate and resulting rupture surfaces (Load Case B).

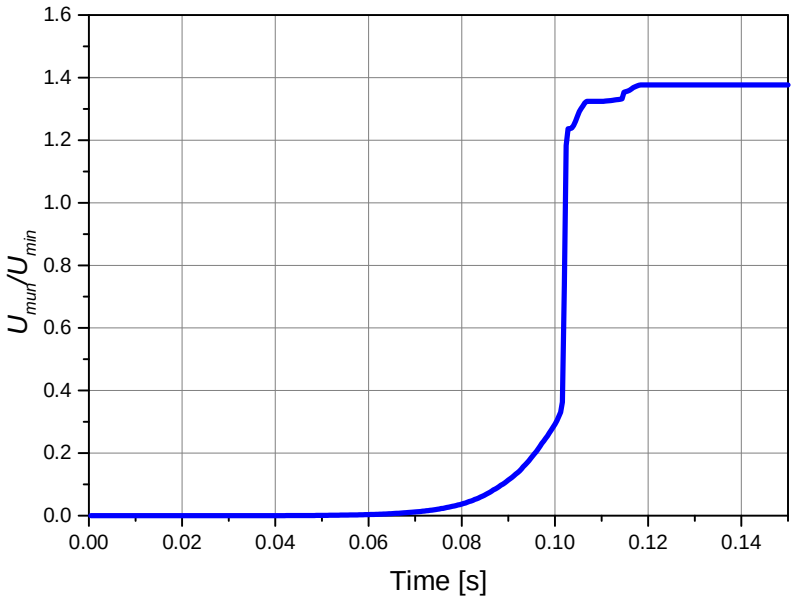


Figure 12: Evolution of $U_{num}/U_{min}$ with time for simulation 1 of 1m plate (Load case B).

Table 3 and Table 4 present all fractal dimension calculated as described above for load case case A and case B) considering all the size plate studied and the three approaches employed to estimated the fractal dimension that is $\Delta_{patch}$ (eq. 24), $\Delta$ ( eq. 27) e $\Delta e$ (eq. 30). Also the results are shown in graphical form in the Figure 13 to Figure 15.

| | | | Sim1 | Sim2 | Sim3 | Sim4 | Sim5 | Sim6 | Mean | σ | CV |
|---|---|---|---|---|---|---|---|---|---|---|---|
| L = 1m | $L_1$ | $\Delta_{patch}$ | 1.047 | 1.084 | 1.030 | 0.702* | 1.039 | 0.782* | 1.050 | 0.024 | 2.25% |
| | | $\Delta$ | 1.062 | 1.109 | 1.039 | 0.612* | 1.050 | 0.716* | 1.065 | 0.031 | 2.89% |
| | $L_2$ | $\Delta_{patch}$ | 1.063 | 1.138 | 1.071 | 0.950* | 1.069 | 1.000 | 1.068 | 0.049 | 4.60% |
| | | $\Delta$ | 1.082 | 1.180 | 1.092 | 0.935* | 1.090 | 1.000 | 1.089 | 0.064 | 5.87% |
| | $\Delta e$ | | 1.116 | 1.165 | 1.101 | 0.999* | 1.099 | 1.089 | 1.114 | 0.030 | 2.72% |
| L = 4m | $L_1$ | $\Delta_{patch}$ | 1.210 | 1.069 | 1.161 | 1.050 | 1.053 | 1.063 | 1.101 | 0.068 | 6.16% |
| | | $\Delta$ | 1.171 | 1.056 | 1.131 | 1.041 | 1.043 | 1.051 | 1.082 | 0.055 | 5.09% |
| | $L_2$ | $\Delta_{patch}$ | 1.265 | 1.089 | 1.175 | 1.068 | 1.065 | 1.093 | 1.126 | 0.079 | 7.03% |
| | | $\Delta$ | 1.215 | 1.072 | 1.142 | 1.055 | 1.053 | 1.075 | 1.102 | 0.064 | 5.83% |
| | $\Delta e$ | | 1.311 | 1.251 | 1.282 | 1.188 | 1.211 | 1.272 | 1.252 | 0.046 | 3.66% |
| L = 8m | $L_1$ | $\Delta_{patch}$ | 1.080 | 1.118 | 1.054 | 1.135 | 1.039 | 1.060 | 1.081 | 0.038 | 3.52% |
| | | $\Delta$ | 1.055 | 1.080 | 1.037 | 1.093 | 1.026 | 1.041 | 1.055 | 0.026 | 2.46% |
| | $L_2$ | $\Delta_{patch}$ | 1.106 | 1.129 | 1.093 | 1.149 | 1.121 | 1.105 | 1.117 | 0.020 | 1.79% |
| | | $\Delta$ | 1.073 | 1.088 | 1.063 | 1.102 | 1.083 | 1.072 | 1.080 | 0.014 | 1.27% |
| | $\Delta e$ | | 1.278 | 1.280 | 1.268 | 1.291 | 1.312 | 1.227 | 1.276 | 0.028 | 2.20% |
| L = 15m | $L_1$ | $\Delta_{patch}$ | 1.057 | 1.162 | 1.221 | 1.069 | 1.260 | 1.082 | 1.142 | 0.086 | 7.51% |
| | | $\Delta$ | 1.034 | 1.097 | 1.132 | 1.041 | 1.155 | 1.049 | 1.085 | 0.051 | 4.73% |
| | $L_2$ | $\Delta_{patch}$ | 1.145 | 1.168 | 1.275 | 1.132 | 1.279 | 1.146 | 1.156 | 0.016 | 1.40% |
| | | $\Delta$ | 1.087 | 1.100 | 1.164 | 1.079 | 1.167 | 1.088 | 1.094 | 0.010 | 0.88% |
| | $\Delta e$ | | 1.345 | 1.289 | 1.374 | 1.299 | 1.362 | 1.326 | 1.317 | 0.040 | 3.03% |

Table 3: Case A: Prescribed boundary displacements.

The values marked with (*) in Table 3 were discarded to compute the statistical values in terms of fractal dimension because in these cases the total fracture of the plate was not achieved in the simulations.

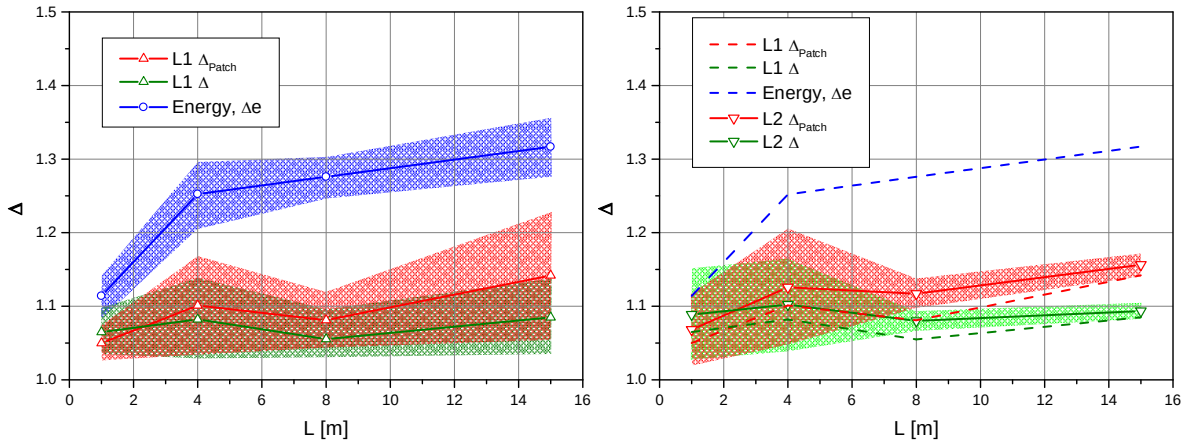


Figure 13: Fractal dimension Δ vs plate size L for prescribed displacements (Case A) showing range of simulated values

| | | | Sim1 | Sim2 | Sim3 | Sim4 | Sim5 | Sim6 | Mean | σ | CV |
|---|---|---|---|---|---|---|---|---|---|---|---|
| L = 1m | $L_1$ | $\Delta_{patch}$ | 1.047 | 1.240 | 1.042 | 1.006 | 1.175 | 1.044 | **1.092** | **0.093** | **8.50%** |
| | | $\Delta$ | 1.062 | 1.313 | 1.054 | 1.008 | 1.228 | 1.057 | **1.120** | **0.121** | **10.78%** |
| | $L_2$ | $\Delta_{patch}$ | 1.095 | 1.305 | 1.102 | 1.099 | 1.223 | 1.148 | **1.162** | **0.085** | **7.34%** |
| | | $\Delta$ | 1.124 | 1.396 | 1.133 | 1.129 | 1.290 | 1.192 | **1.211** | **0.111** | **9.16%** |
| | $\Delta e$ | | 1.139 | 1.357 | 1.151 | 1.138 | 1.268 | 1.174 | **1.205** | **0.089** | **7.40%** |
| L = 4m | $L_1$ | $\Delta_{patch}$ | 1.015 | 1.141 | 1.236 | 1.053 | 1.053 | 1.296 | **1.132** | **0.113** | **10.00%** |
| | | $\Delta$ | 1.012 | 1.114 | 1.192 | 1.043 | 1.043 | 1.240 | **1.107** | **0.092** | **8.30%** |
| | $L_2$ | $\Delta_{patch}$ | 1.229 | 1.229 | 1.272 | 1.112 | 1.104 | 1.527 | **1.246** | **0.154** | **12.37%** |
| | | $\Delta$ | 1.186 | 1.186 | 1.221 | 1.091 | 1.084 | 1.428 | **1.199** | **0.125** | **10.43%** |
| | $\Delta e$ | | 1.297 | 1.309 | 1.330 | 1.202 | 1.221 | 1.474 | **1.305** | **0.097** | **7.43%** |
| L = 8m | $L_1$ | $\Delta_{patch}$ | 1.088 | 1.307 | 1.178 | 1.112 | 1.047 | 1.197 | **1.155** | **0.093** | **8.08%** |
| | | $\Delta$ | 1.060 | 1.210 | 1.122 | 1.076 | 1.032 | 1.135 | **1.106** | **0.064** | **5.77%** |
| | $L_2$ | $\Delta_{patch}$ | 1.154 | 1.358 | 1.247 | 1.318 | 1.147 | 1.326 | **1.258** | **0.091** | **7.23%** |
| | | $\Delta$ | 1.105 | 1.244 | 1.169 | 1.218 | 1.101 | 1.223 | **1.177** | **0.062** | **5.29%** |
| | $\Delta e$ | | 1.286 | 1.343 | 1.307 | 1.324 | 1.318 | 1.284 | **1.311** | **0.023** | **1.74%** |
| L = 15m | $L_1$ | $\Delta_{patch}$ | 1.177 | 1.016 | 1.057 | 1.057 | 1.065 | 1.101 | **1.079** | **0.055** | **5.11%** |
| | | $\Delta$ | 1.106 | 1.009 | 1.034 | 1.034 | 1.039 | 1.060 | **1.047** | **0.033** | **3.15%** |
| | $L_2$ | $\Delta_{patch}$ | 1.236 | 1.226 | 1.132 | 1.289 | 1.108 | 1.149 | **1.190** | **0.071** | **5.93%** |
| | | $\Delta$ | 1.141 | 1.135 | 1.079 | 1.173 | 1.065 | 1.089 | **1.114** | **0.042** | **3.79%** |
| | $\Delta e$ | | 1.359 | 1.260 | 1.294 | 1.311 | 1.279 | 1.321 | **1.304** | **0.035** | **2.66%** |

Table 4: Case B: Prescribed force.

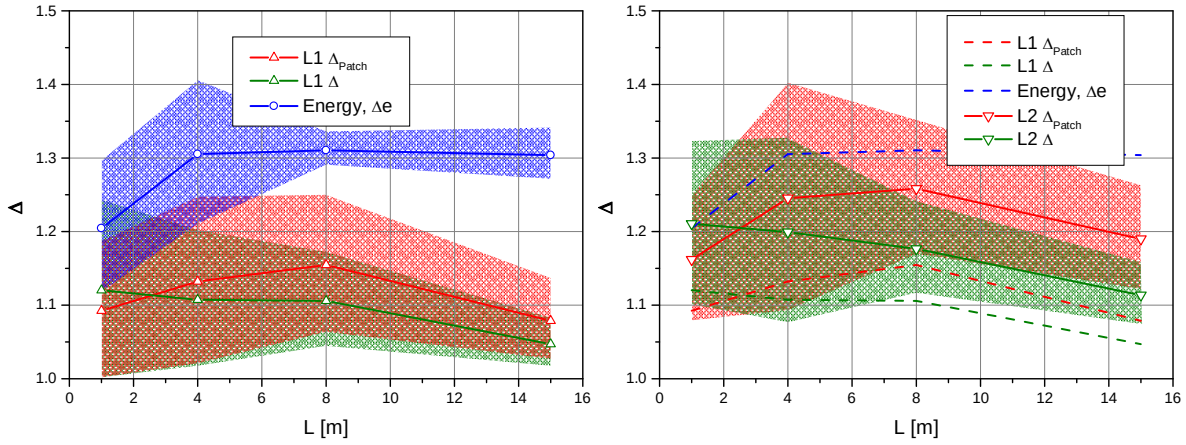


Figure 14: Fractal dimension Δ *vs* plate size L for prescribed boundary forces (Case B) showing range of simulated values.

The numerical results presented herein require further evaluation. Some observations may however be advanced at the present stage. The apparent dependence of the fractal dimension on the plate size, which tends to dissapear for larger sizes, may be due to the coarse modelling adopted for the smaller plates.

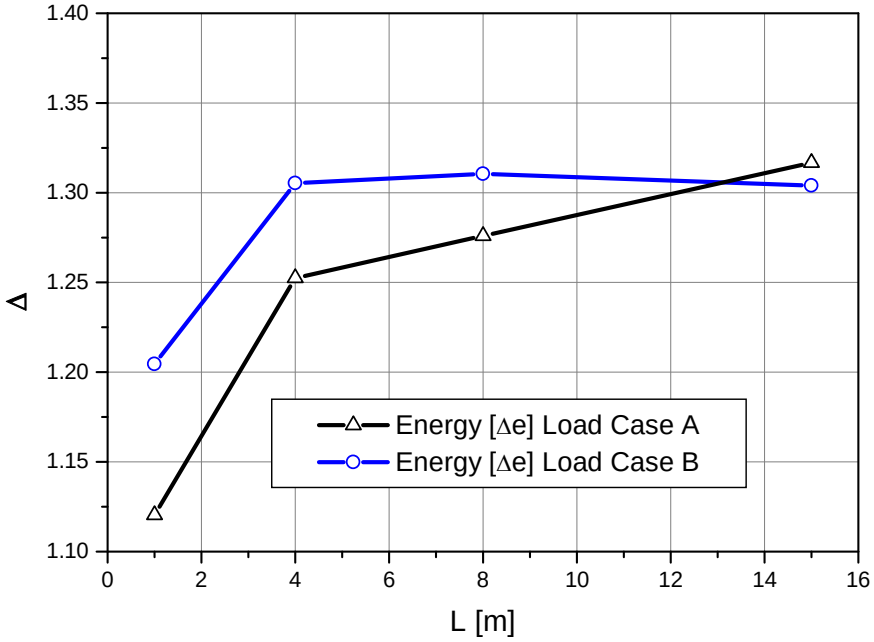


Figure 15: Fractal exponents according to Method 3 for Cases A and B *vs* plate size.

## 7 CONCLUSIONS

The numerical analysis of plates subjected to tensile fracture employing the truss-like discrete element method (DEM) is initially described in the paper. Various approaches to determine the fractal dimension of the fractured area are examined next. In this context, the authors resort to the notion of fractal dimension proposed by Carpinteri within the Fracture Mechanics Theory of quasi fragile materials. It is tentatively concluded that the three methods employed to compute de fractal dimension led to credible results but their applicability end efficiency demand additional experimentation. Moreover, a perceptible trend for damage concentration in a single fissure for applied loads in relation to applied displacements was detected in the simulations.

**Acknowledgements:** The authors acknowledge the support of CNPq and CAPES (Brazil).

## REFERENCES

Carpinteri A., 1994. Scaling laws and renormalization groups for strength and toughness of disordered materials. *Int. J, Solids Struct*. 31, 291-302.

Carpinteri A., Chiapa B., Invernizzi S., 1999. Three-dimensional fractal analysis of concrete fracture at the meso-level. *Theoretical and Applied Fracture Mechanics*, 31, 163-172.

Clarke K.C., 1986. Computation of the fractal dimension of topographic surfaces using the triangular prism surface area method. *Computer and Geosciences* 12. 713-722.

Dalguer L.A., Irikura K., Riera J.D. and Chiu H.C., 2001. The importance of the dynamic source effects on strong ground motion during the 1999 Chi-Chi, Taiwan, earthquake: Brief interpretation of the damage distribution on buildings. *Bull. Seismol. Soc. Am.*, 91, 1112-1127.

Hillerborg A., 1978. A Model for Fracture Analysis. Cod LUTVDG/TV BM-3005/1-8.

Hayashi Y., 1982. Sobre uma representação discreta de meios contínuos em dinâmica não-linear. M. S. thesis, CPGEC, Universidade Federal do Rio Grande do Sul, Porto Alegre, Brazil.

Mandelbrot B.B., 1982. *The Fractal Geometry of Nature*. Freeman, San Francisco.

Miguel, L.F.F., Iturrioz I., Riera J.D., 2010. Size effects and mesh independence in dynamic fracture analysis of brittle materials. *CMES*, vol.56, no.1, pp.1-16.

Nayfeh A.H. and Hefzy M.S., 1978. Continuum modeling of three-dimensional truss-like space structures. *AIAA Journal*, 16(8), 779-787.

Riera J.D. and Rocha M.M., 1991. A note on velocity of crack propagation in tensile fracture. Revista Brasileira de Ciências Mecânicas. Vol. XII/3, pp. 217-240.

Rocha M.M., 1989. Ruptura e Efeitos de Escala em Materiais não Homogêneos. M. S. thesis, CPGEC, Universidade Federal do Rio Grande do Sul, Porto Alegre, Brazil.

Rocha M.M., Riera J.D., Krutzik N.J., 1991. Extension of a model that aptly describes fracture of plain concrete to the impact analysis of reinforced concrete. *Int. Conf. and Structural Mechanics in Reactor Technology*, SMiRT 11, Trans. Vol. J., Tokyo, Japan.

Turcotte D.L., 1992. Fractal and Chaos in Geology and Geophysics. Cambridge University Press, Cambridge.